



iPLA2 β -mediated lipid detoxification controls p53-driven ferroptosis independent of GPX4

Delin Chen^{1,5}, Bo Chu^{1,5}, Xin Yang¹, Zhaoqi Liu², Ying Jin¹, Ning Kon¹, Raul Rabadan ², Xuejun Jiang ³, Brent R. Stockwell⁴ & Wei Gu ¹✉

Here, we identify iPLA2 β as a critical regulator for p53-driven ferroptosis upon reactive oxygen species (ROS)-induced stress. The calcium-independent phospholipase iPLA2 β is known to cleave acyl tails from the glycerol backbone of lipids and release oxidized fatty acids from phospholipids. We found that iPLA2 β -mediated detoxification of peroxidized lipids is sufficient to suppress p53-driven ferroptosis upon ROS-induced stress, even in GPX4-null cells. Moreover, iPLA2 β is overexpressed in human cancers; inhibition of endogenous iPLA2 β sensitizes tumor cells to p53-driven ferroptosis and promotes p53-dependent tumor suppression in xenograft mouse models. These results demonstrate that iPLA2 β acts as a major ferroptosis repressor in a GPX4-independent manner. Notably, unlike GPX4, loss of iPLA2 β has no obvious effect on normal development or cell viability in normal tissues but iPLA2 β plays an essential role in regulating ferroptosis upon ROS-induced stress. Thus, our study suggests that iPLA2 β is a promising therapeutic target for activating ferroptosis-mediated tumor suppression without serious toxicity concerns.

¹Institute for Cancer Genetics, and Department of Pathology and Cell Biology, and Herbert Irving Comprehensive Cancer Center, Vagelos College of Physicians & Surgeons, Columbia University, New York, NY 10032, USA. ²Program for Mathematical Genomics, Departments of Systems Biology and Biomedical Informatics, Columbia University, New York, NY 10032, USA. ³Cell Biology Program, Memorial Sloan-Kettering Cancer Center, New York, NY 10065, USA. ⁴Department of Biological Sciences, Department of Chemistry, Columbia University, New York, NY 10027, USA. ⁵These authors contributed equally: Delin Chen, Bo Chu. ✉email: wg8@cumc.columbia.edu

Inactivation of the p53 tumor suppressor is a pivotal event in the formation of most human cancers. p53 plays a central role by acting as a transcription factor to modulate various types of cellular processes to suppress cancer development^{1,2}. Among the multiple layers of mechanisms controlling p53 function, negative regulators in modulating p53 responses such as Mdm2/Mdmx oncoproteins are particularly interesting as these factors act as potential targets for activating p53 function in cancer therapy^{3,4}. The exquisite regulation of p53 functions is of vital importance for cell fate decisions. Although the classic activities of p53 including cell cycle arrest, apoptosis, and senescence are well accepted as the major mechanisms in tumor suppression, recent studies suggest that unconventional mechanisms also contribute significantly to tumor suppression^{5,6}. We and others recently found that p53 plays an important role in modulating ferroptotic cell death responses in cancer cells through its metabolic targets^{7–11}.

Ferroptosis is an iron-dependent form of non-apoptotic cell death induced by excess accumulation of peroxidized phospholipids, generated through oxidation of the polyunsaturated fatty acyl (PUFA) moieties of membrane phospholipids^{12–14}. Ferroptosis under normal homeostasis conditions is tightly controlled by glutathione peroxidase 4 (GPX4), which converts lipid hydroperoxides into non-toxic lipid alcohols^{15,16}. Recent studies indicate that ferroptosis, like apoptosis acts as a new tool for suppressing tumor growth; inhibitors of GPX4 have been proposed as promising drugs in cancer therapy^{17–19}. Ferroptosis induced by GPX4 inhibition is dependent on the activity of acyl-CoA synthetase long-chain family member 4 (ACSL4), which incorporates free fatty acids such as PUFAs into phospholipids (PL-PUFAs)^{20,21}. Thus, the cells lacking ACSL4 expression are resistant to ferroptosis induced by GPX4 inhibitors²⁰. We and others found that the ability of p53 to induce ferroptosis significantly contributes to its tumor suppression activity^{7,8,22}. Notably, p53-mediated ferroptosis acts mainly through the ALOX12 lipoxygenase upon reactive oxygen species (ROS)-induced stress¹¹. The ALOX12 gene resides on human chromosome 17p13.1 at a common position with frequent monoallelic deletion in human cancers. Indeed, loss of one ALOX12 allele is sufficient to accelerate tumorigenesis by abrogating p53-mediated ferroptosis and tumor suppression in mouse lymphoma models. Surprisingly, however, ALOX12 is dispensable for ferroptosis induced by GPX4 inhibitors, whereas ACSL4 is not required for p53-mediated ferroptosis upon ROS-induced stress¹¹. These studies suggest that p53 promotes ferroptosis through a distinct GPX4-independent pathway critically for its tumor suppression. Moreover, it remains unclear whether any GPX4-like factor is involved in regulating p53-dependent ferroptosis and tumor suppression. Here, we identify iPLA2 β as a major suppressor of p53-mediated ferroptosis in the cells subjected to ROS-induced stress. We demonstrate that iPLA2 β -mediated detoxification of peroxidized lipids is sufficient to suppress p53-driven ferroptosis in a GPX4-independent manner. Moreover, depletion of endogenous iPLA2 β sensitizes tumor cells to ROS-induced ferroptosis and enhances p53-dependent tumor growth suppression. Thus, our results indicate that iPLA2 β -mediated lipid detoxification is critically involved in suppressing p53-mediated ferroptosis and tumor suppression and suggest that iPLA2 β is a promising target for activating ferroptosis in human cancers.

Results

p53-Driven ferroptosis is induced in a GPX4-independent manner. We previously established that p53-dependent ferroptosis can be induced in the presence of elevated levels of ROS, generated by *tert*-Butyl hydroperoxide (TBH) without common

ferroptosis inducers such as erastin or GPX4 inhibitors⁷. Although no significant cell death was observed under low levels of TBH treatment in human cancer cells, the combination of TBH treatment and p53 activation (e.g., Nutlin treatment) is able to effectively induce high levels of ferroptosis, even in ACSL4-null cells¹¹. Since ACSL4 is essential for ferroptosis induced by GPX4 inhibitors^{20,21}, it is likely that p53-mediated ferroptotic response is independent of GPX4 function. However, this notion cannot be directly tested since GPX4-null cells do not survive under normal conditions unless ACSL4 is co-deleted. To address whether p53-mediated ferroptosis can be induced independent of GPX4 function, we generated ACSL4/GPX4 double-knockout derivatives of the human osteosarcoma cell line U2OS. As shown in Fig. 1a, the levels of p53 were unaffected by loss of ACSL4 and GPX4 and, p53-mediated transcription activation of p21 or p53-mediated repression of SLCTA11 remained intact. Also, given their lack of ACSL4, these cells are resistant to ferroptosis induced by either erastin (Fig. 1b) or the GPX4 inhibitor RSL-3 (Fig. 1c). However, ferroptotic cell death was readily observed when ACSL4/GPX4-null cells were exposed to both the ROS generator TBH and the p53 activator Nutlin (Fig. 1d and Supplementary Fig. 1a). As expected, the levels of ferroptosis were largely abrogated when isogenic p53-null, or ALOX12-null U2OS cells were subjected to the same conditions (Supplementary Fig. 1a, b). Similar results were also obtained with independent ACSL4/GPX4-null clones (Supplementary Fig. 2a, b). Moreover, these p53-mediated responses were specifically blocked by known ferroptosis inhibitors (e.g., Ferr-1, DFO, and Lipro-1) but not by inhibitors of other cell death pathways, such as apoptosis, autophagy or necroptosis (Fig. 1d). Similar results were reproduced when an independent cell death assay was used by monitoring cellular ATP levels (Supplementary Fig. 2c).

Next, we examined whether p53-mediated ferroptosis can be elicited by other ROS-generating compounds, such as DDM-9,2-butanone peroxide (BTP) and cumene hydroperoxide (CMH) with very similar chemical structures compared to TBH (Fig. 2a). Indeed, both compounds readily induced high levels of ferroptosis in both parental and ACSL4/GPX4-null U2OS cells under the same conditions (Fig. 2b, c). Moreover, elevated levels of endogenous lipid peroxidation, a key marker of ferroptosis, were observed by flow cytometry with C11-BODIPY staining when either parental or ACSL4/GPX4-null cells were treated with both Nutlin and TBH (Fig. 2d, e). Taken together, these data demonstrate that p53-driven ferroptosis upon high levels of ROS is induced in a GPX4-independent manner.

iPLA2 β is differentially regulated by p53 upon different levels of stress. Under normal homeostasis conditions, GPX4 protects cells from ferroptosis by converting oxidized phospholipids into non-toxic lipid alcohols^{15–17}. However, our results indicate that, under conditions of oxidative stress, p53-mediated ferroptosis is independent of GPX4 activity. Thus, we considered whether other modes of lipid detoxification are involved in regulating p53-mediated ferroptosis. Phospholipases can cleave the glycerol backbone of phospholipids to yield free fatty acids and lysophospholipids²³. Moreover, recent studies have shown that the calcium-independent phospholipase iPLA2 γ is able to hydrolyze oxidized cardiolipin (CL), an inner mitochondrial membrane phospholipid and, subsequently release oxidized fatty acids from cardiolipin^{24–26}. Interestingly, upon analysis of our RNA-Seq data, we found that the mRNA levels of iPLA2 β , another member of the calcium-independent phospholipase A2 family, were induced by p53 activation.

To ascertain whether the iPLA2 β gene is indeed regulated by p53, we examined iPLA2 β expression in response to p53

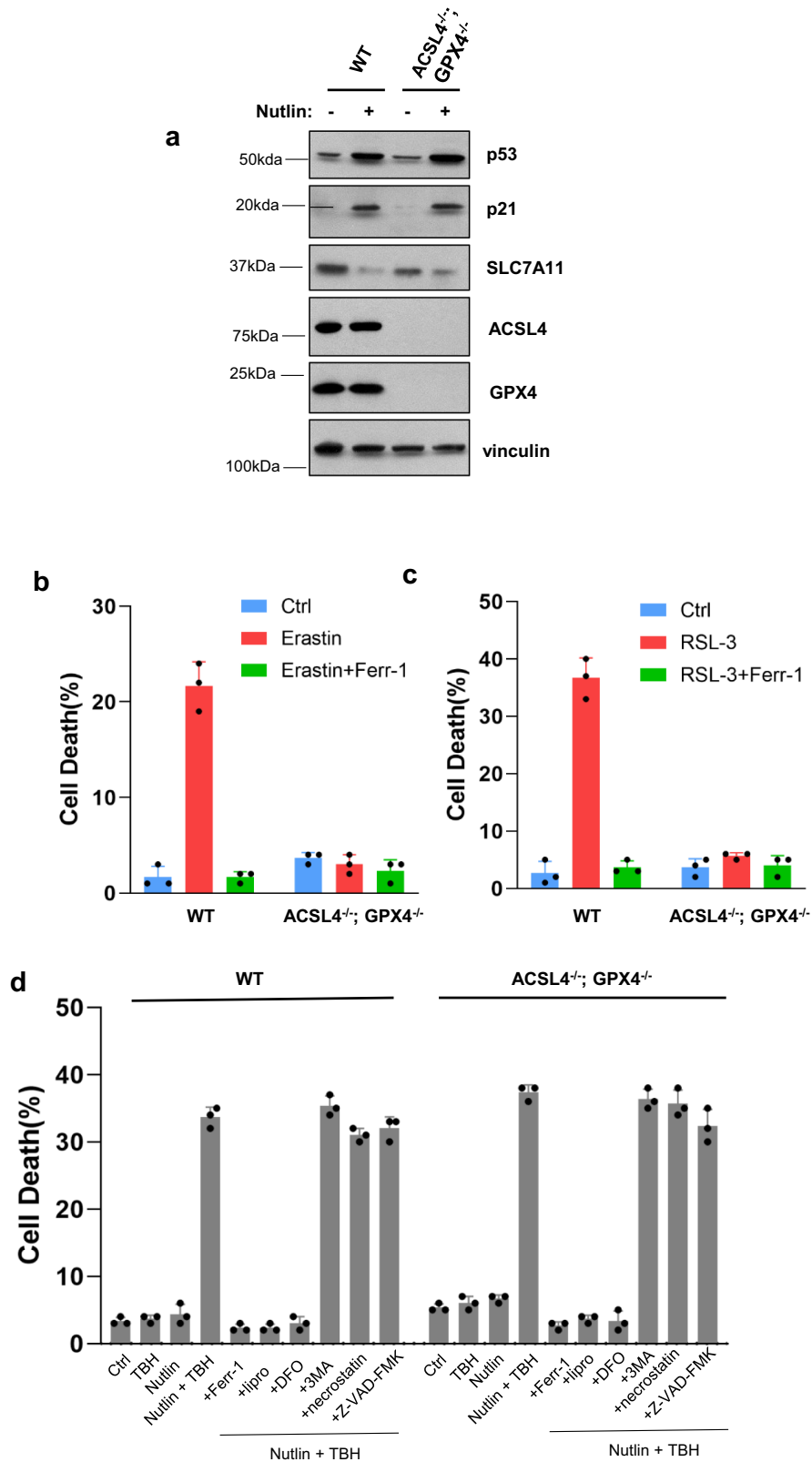


Fig. 1 p53-Mediated ferroptosis is GPX4-independent upon ROS-induced stress. **a** Western blot analysis of U2OS ACSL4^{-/-}; GPX4^{-/-} cells treated with Nutlin (10 μM) as indicated for 48 h. The experiments were repeated twice, independently, with similar results. **b** U2OS ACSL4^{-/-}; GPX4^{-/-} cells were treated with Erastin (40 μM) and Ferr-1 (2 μM) as indicated for 12 h. **c** U2OS ACSL4^{-/-}; GPX4^{-/-} cells were treated with RSL-3 (2 μM) and Ferr-1 (2 μM) as indicated for 12 h. **d** U2OS control, ACSL4^{-/-}; GPX4^{-/-} cells pre-incubated with Nutlin (10 μM) for 24 h were treated with TBH (250 μM), Nutlin (10 μM), Ferr-1 (2 μM), Lipro-1 (2 μM), 3-MA (2 mM), necrostatin-1 (10 μg/mL), and Z-VAD-FMK (10 μg/mL) as indicated, for 8 h. 3-MA, 3-methyladenine. **b-d** Error bars are mean ± s.d., n = 3 biologically independent experiments. Source data are provided as a Source Data file.

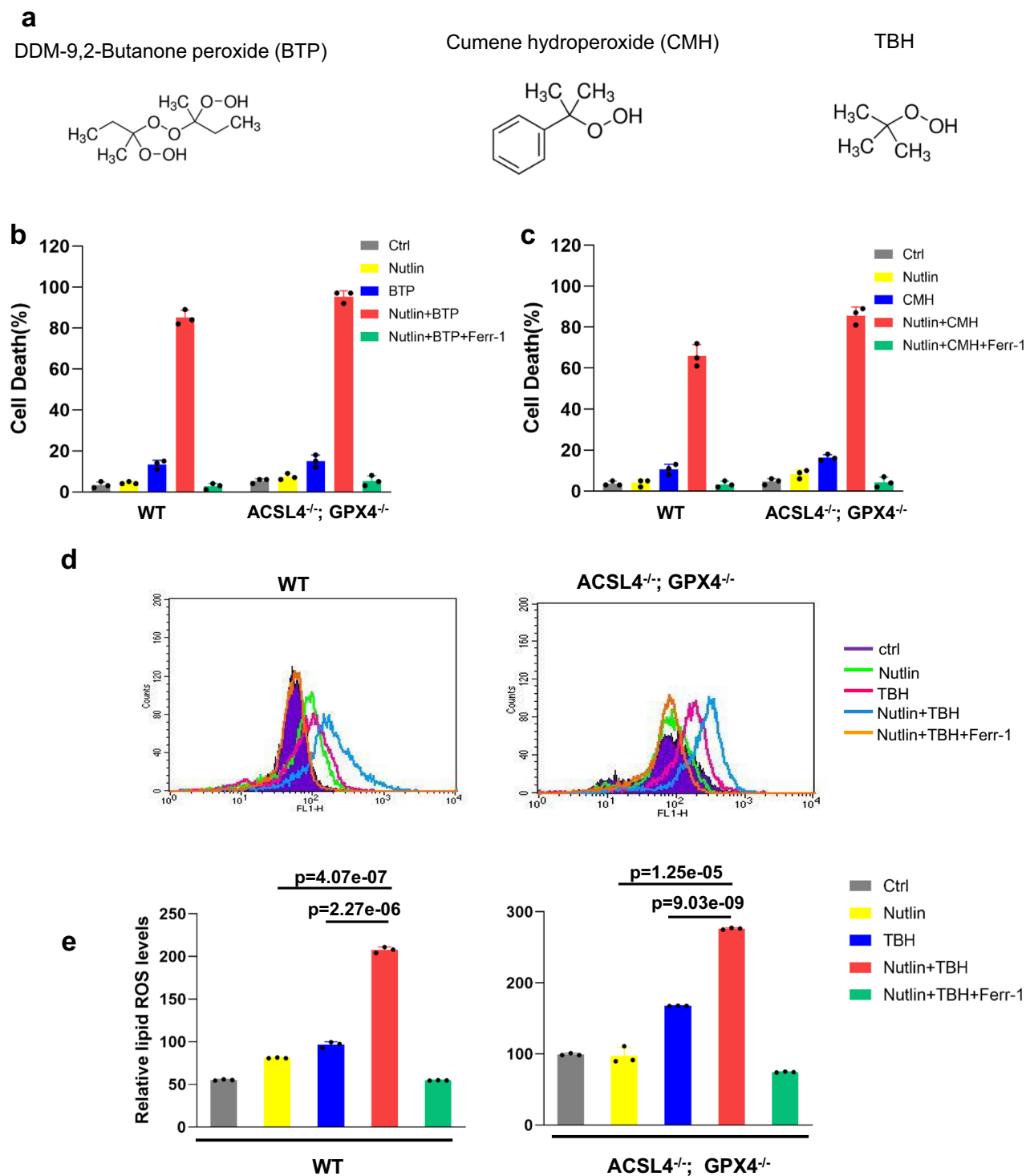


Fig. 2 BTP or CMH has similar effects as TBH does. **a** Variant compounds having similar functional group with TBH. **b** U2OS control, ACSL4^{-/-}; GPX4^{-/-} cells pre-incubated with Nutlin (10 μ M) for 12 h were treated with BTP (300 μ M), Nutlin (10 μ M), and Ferr-1 (2 μ M) as indicated for 8 h. BTP, butanone peroxide. **c** U2OS control, ACSL4^{-/-}; GPX4^{-/-} cells pre-incubated with Nutlin (10 μ M) for 12 h were treated with CMH (200 μ M), Nutlin (10 μ M), and Ferr-1 (2 μ M) as indicated for 8 h. CMH, cumene hydroperoxide. **d** Lipid peroxidation levels of U2OS control, ACSL4^{-/-}; GPX4^{-/-} cells pre-incubated with Nutlin (10 μ M) for 12 h were treated with TBH (300 μ M), Nutlin (10 μ M), and Ferr-1 (2 μ M) as indicated for 8 h. **e** Quantification of lipid peroxidation levels is shown as in (d). **b, c, e** Error bars are mean \pm s.d., $n = 3$ independent repeats. **e** All p values were calculated using two-tailed unpaired Student's t -test. Detailed statistical tests are described in the 'Methods'. For WT, $p = 0.000000227$, TBH versus Nutlin + TBH; $p = 0.0000000407$, Nutlin versus Nutlin + TBH. For ACSL4^{-/-}; GPX4^{-/-}, $p = 0.00000000903$, TBH versus Nutlin + TBH; $p = 0.00000125$, Nutlin versus Nutlin + TBH. Source data are provided as a Source Data file.

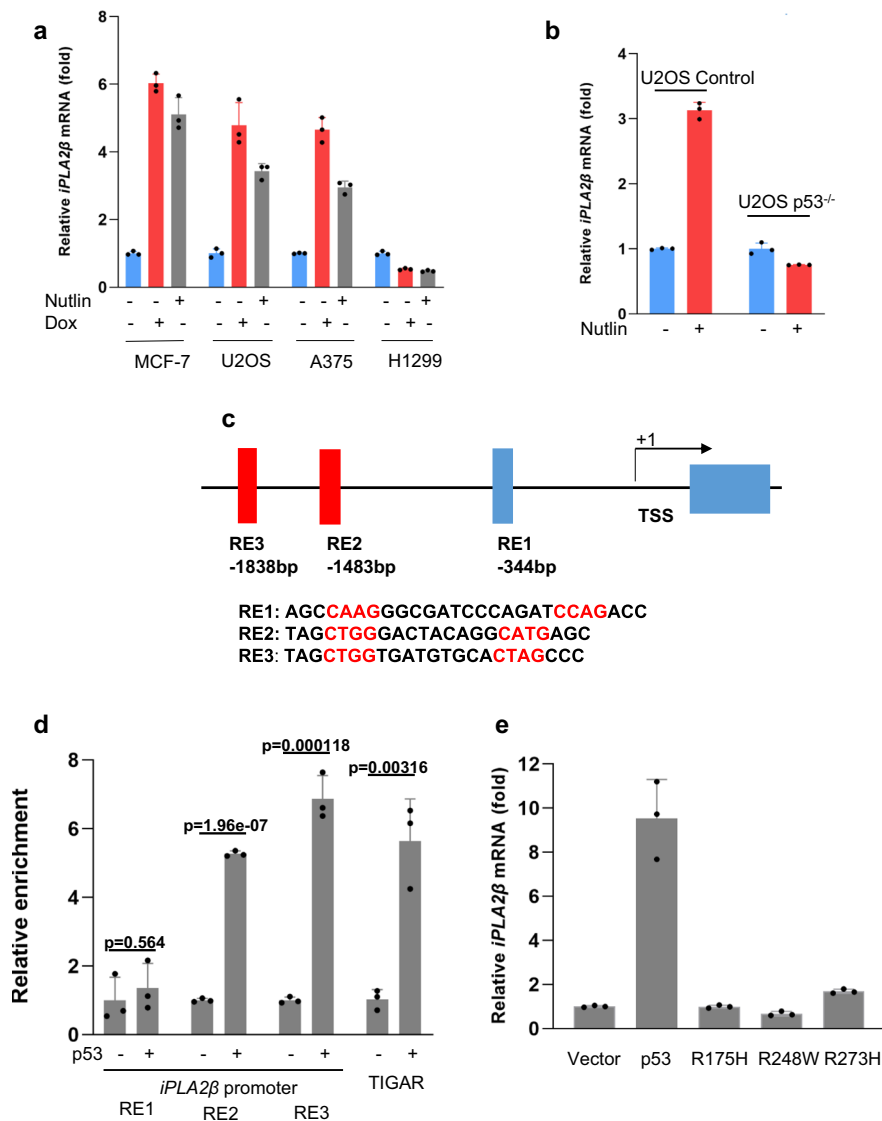


Fig. 3 Regulation of *iPLA2β* during p53-mediated stress responses. **a** qPCR analysis of mRNA levels of *iPLA2β* in the MCF-7, U2OS, A375, and H1299 cells treated with 0.2 μg/mL doxorubicin or 10 μM Nutlin for 24 h. **b** qPCR analysis of mRNA levels of *iPLA2β* in the U2OS CRISPR control versus p53^{-/-} cells treated with 10 μM Nutlin for 24 h. **c** Schematic representation of the promoter region in the human *iPLA2β* gene. The p53-binding sites upstream of the first exon are indicated as responsive elements (RE). TSS, transcription start site. **d** ChIP-qPCR was performed in H1299 cells transfected with empty vector or p53. *p* values were calculated using two-sided unpaired Student's *t*-test. Detailed statistical tests are described in the 'Methods'. *p* = 0.564 for RE1; *p* = 0.000000196 for RE2; *p* = 0.000118 for RE3; and *p* = 0.00316 for TIGAR. **e** H1299 cells were transfected with empty vector, wild-type p53 or mutants (R175H, R273H, and R248W), and *iPLA2β* mRNA levels were analyzed by qRT-PCR. **a**, **b**, **d**, **e** Error bars are mean ± s.d., *n* = 3 biologically independent experiments. Source data are provided as a Source Data file.

activation by either Nutlin or doxorubicin, a common DNA damage reagent. *iPLA2β* mRNA levels were modestly but significantly upregulated by treatment with either Nutlin or doxorubicin in cell lines that express wild-type p53 (U2OS, MCF7, A375, A549 cells), but not in the p53-null line H1299 (Fig. 3a and Supplementary Fig. 3). To confirm that *iPLA2β* transcription is dependent on p53, we also evaluated U2OS sublines generated by CRISPR-mediated inactivation of the p53 gene. As shown in Fig. 3b, the mRNA levels of *iPLA2β* were induced by Nutlin treatment in parental, but not p53-knockout, cells. Furthermore, the promoter region of the human *iPLA2β* gene contains three potential sites (RE1, RE2, and RE3) that match the consensus p53-binding sequence (Fig. 3c). Indeed, chromatin immunoprecipitation (ChIP) analysis with a p53-specific antibody revealed significant recruitment of p53 to RE2 and RE3, but not RE1, at levels comparable to those observed at

the promoter of TIGAR²⁷, a well-known metabolic target of p53 (Fig. 3d). Of note, *iPLA2β* mRNA expression was readily induced when p53-null H1299 cells were reconstituted by transient transfection with wild-type p53, but not with three tumor-derived DNA-binding defective p53 mutants (R175H, R273H, and R248W) (Fig. 3e).

To further understand the nature of this regulation, we examined the levels of *iPLA2β* under different lengths or different dosages of the same treatments during p53-mediated responses. Notably, the levels of *iPLA2β* were induced at earlier time points but the activation was completely abrogated at a later time point after Nutlin treatment (Fig. 4a, b); conversely, p53-mediated regulation of p21 were observed at all different of time points (Fig. 4a). Since our previous studies showed that p53-mediated regulation of SLC7A11 is critical for ferroptosis^{7,11}, we also monitored the levels of SLC7A11. Indeed, downregulation of

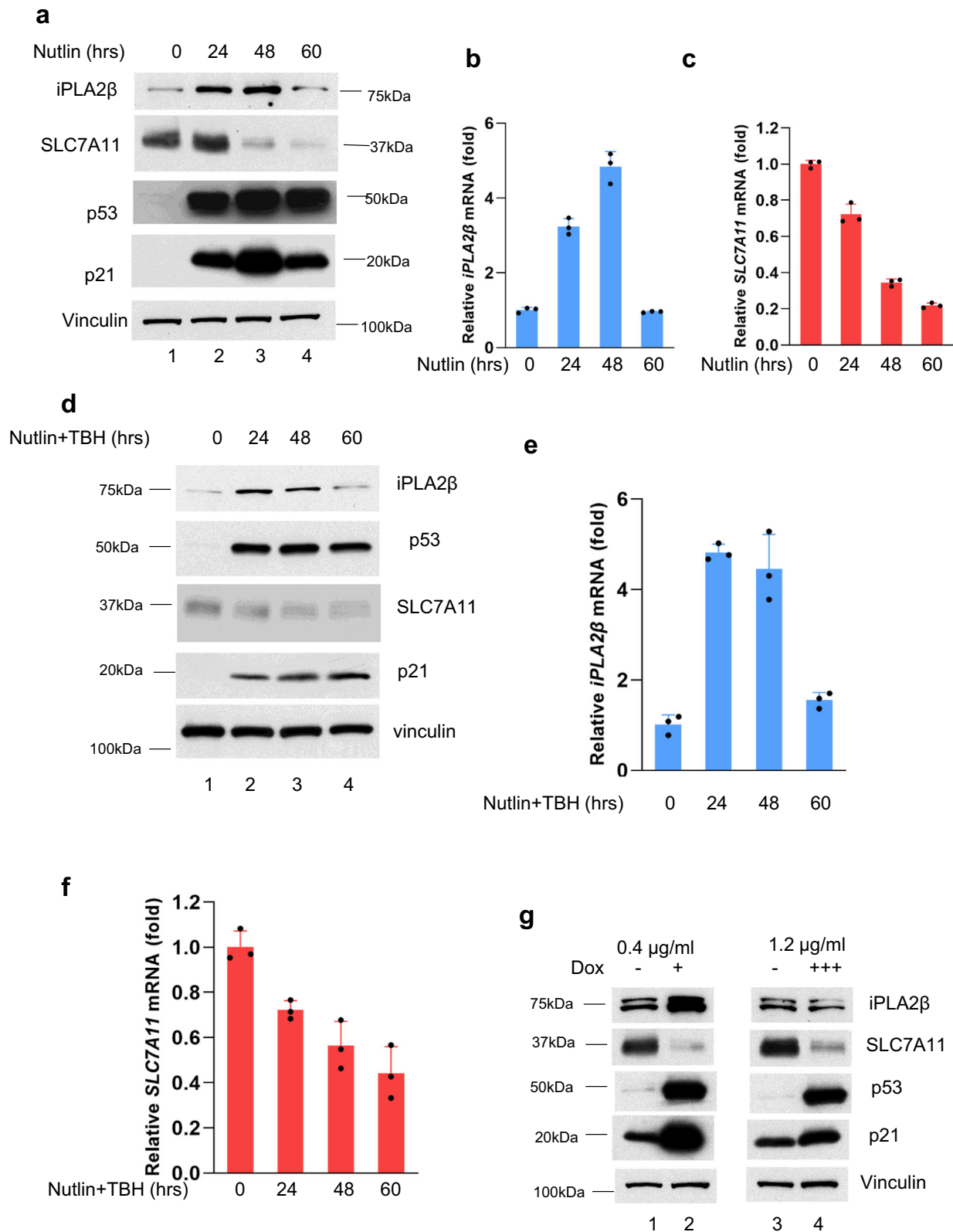
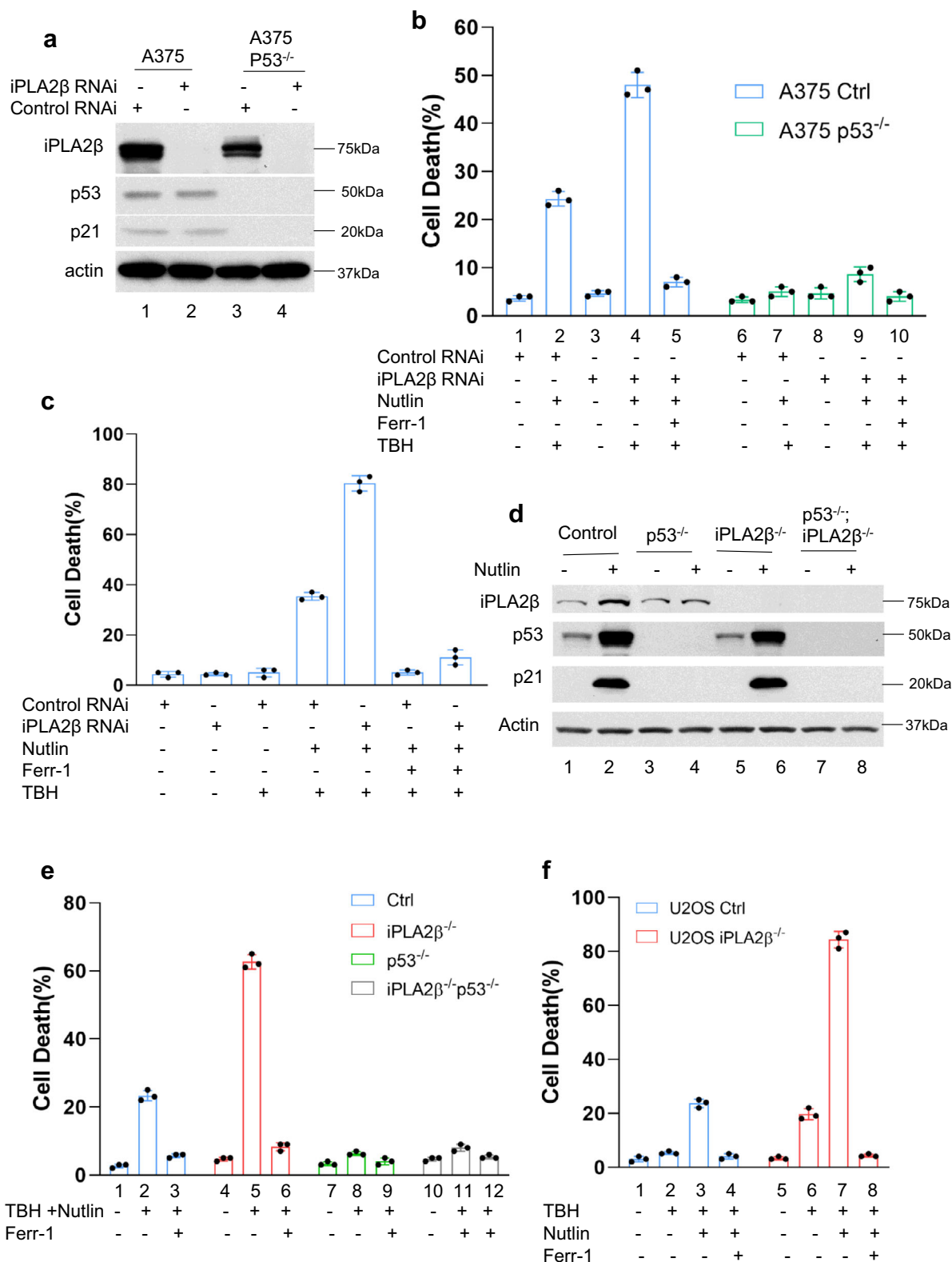


Fig. 4 Differential effects on iPLA2 β mediated by p53 depends on stress duration and intensity. **a** Western blot analysis of extracts of U2OS cells with different time of 10 μ M Nutlin treatment. The experiments were repeated twice, independently, with similar results. **b** qPCR analysis of mRNA levels of *iPLA2 β* for the above cells. **c** qPCR analysis of mRNA levels of *SLC7A11* for the same cells as **(a)**. **d** Western blot analysis of extracts of U2OS cells with different time of 10 μ M Nutlin + TBH treatment. The experiments were repeated twice, independently, with similar results. **e** qPCR analysis of mRNA levels of *iPLA2 β* for the same cells as **(d)**. **f** qPCR analysis of mRNA levels of *SLC7A11* for the same cells as **(d)**. **g** Western blot analysis of extracts of HCT116 cells with low dose (lanes 1, 2) or high dose of doxorubicin (lanes 3, 4) as indicated for 30 h. The experiments were repeated twice, independently, with similar results. **b, c, e, f** Error bars are mean \pm s.d., $n = 3$ biologically independent experiments. Source data are provided as a Source Data file.



SLC7A11 by p53 remained intact at all different of time points (Fig. 4a–c). Similar data were also obtained when the cells were treated with both Nutlin and TBH (Fig. 4d–f), as p53-mediated ferroptosis was examined upon the treatment of both Nutlin and TBH.

Moreover, the levels of iPLA2 β were induced upon a low dose of the DNA damage reagent but the activation was largely abrogated with a high dose of the same reagent in HCT116 cells,

whereas p53-mediated regulation of SLC7A11 and p21 remained intact under both conditions (Fig. 4g). In addition to HCT116 cells, we also performed the same treatment in both U2OS cells and A549 cells. Indeed, similar results were obtained to support the same conclusion (Supplementary Fig. 4a–i). Taken together, although the precise mechanism of p53-mediated transactivation of iPLA2 β needs further elucidation, these data suggest that iPLA2 β is a direct target of p53 but p53-mediated regulation of

Fig. 5 iPLA2 β acts as a major suppressor of p53-mediated ferroptosis. **a** Western blot analysis of extracts of A375 CRISPR control (lanes 1, 2) versus p53^{-/-} cells (lanes 3, 4) treated with control RNAi (lanes 1, 3) or iPLA2 β RNAi (lanes 2, 4) by the antibodies to iPLA2 β , p53, p21, or actin. The experiments were repeated twice, independently, with similar results. **b** Quantification of ROS-induced ferroptotic cell death. The same cells in **(a)** were pre-incubated with 10 μ M Nutlin for 24 h, then treated with 120 μ M TBH and 10 μ M Nutlin (error bars, s.d. from three independent samples). **c** Quantification of ferroptotic cell death-mediated by ROS. After iPLA2 β RNAi treatment, MCF-7 cells were pre-incubated with 10 μ M Nutlin for 24 h, then treated with 80 μ M TBH and 10 μ M Nutlin (error bars, s.d. from three independent samples). **d** Western blot analysis of extracts of A375 CRISPR control (lanes 1, 2), p53^{-/-} cells (lanes 3, 4), iPLA2 β ^{-/-} cells (lanes 5, 6), or p53^{-/-}; iPLA2 β ^{-/-} cells treated with Nutlin 10 μ M for 24 h (lanes 2, 4, 6, 8) versus control (lanes 1, 3, 5, 7) by the antibodies to iPLA2 β , p53, p21, or actin. The experiments were repeated twice, independently, with similar results. **e** Quantification of cell death in the same cells as **(d)** with additional of 150 μ M TBH as indicated. Error bars are mean \pm s.d., $n = 3$ biologically independent experiments. **f** Quantification of ROS-mediated ferroptotic cell death. U2OS CRISPR control versus iPLA2 β ^{-/-} cells pre-incubated with Nutlin (10 μ M) for 24 h were treated with TBH (250 μ M), Nutlin (10 μ M) and Ferr-1 (2 μ M) as indicated (error bars, s.d. from three independent replicates). Source data are provided as a Source Data file.

iPLA2 β is very sensitive to the conditions of the treatment. Indeed, iPLA2 β is activated by p53 at the early stage of stress responses or under low levels of stress but this activation is diminished at the late stage of stress responses or under high levels of stress.

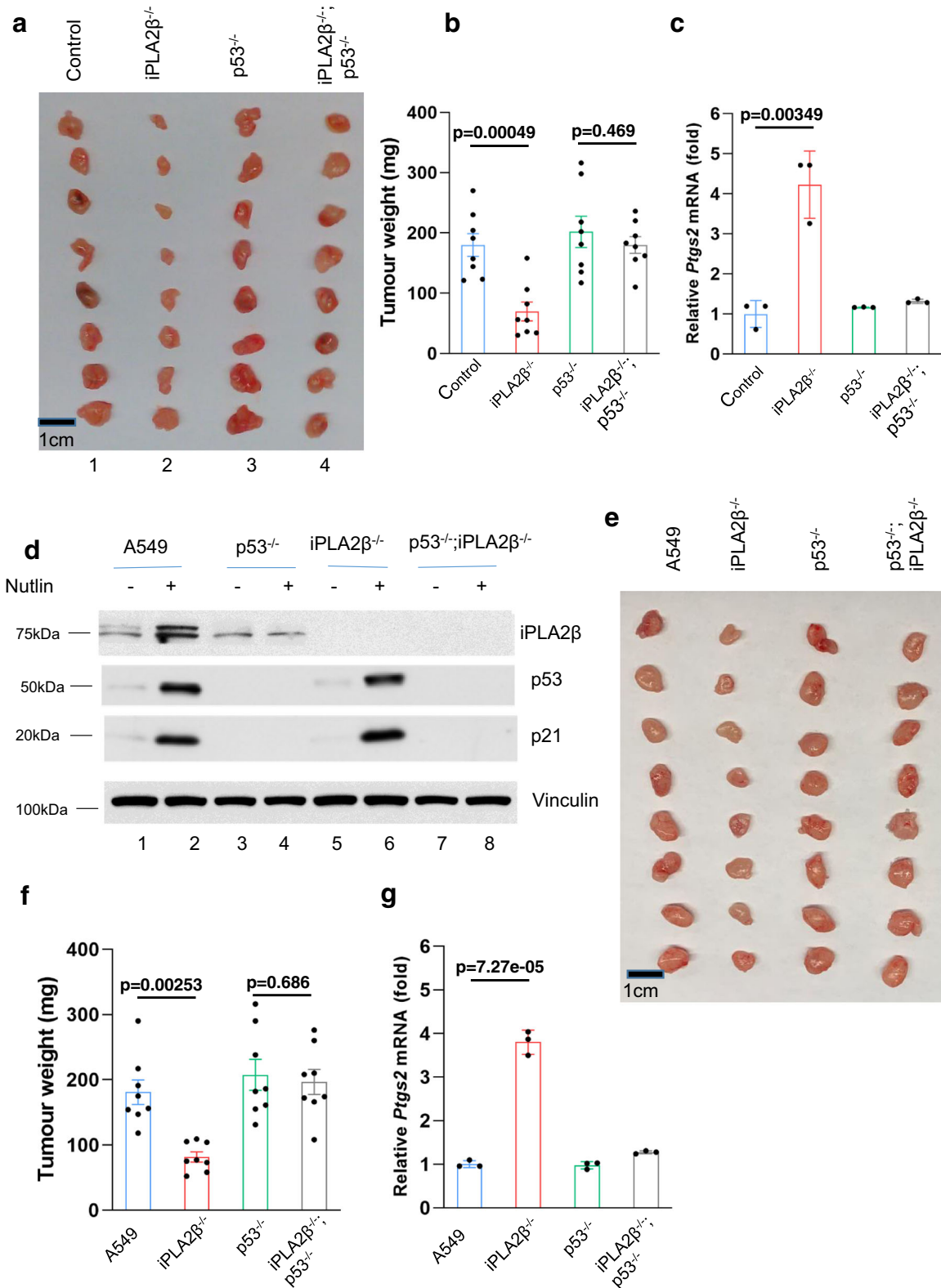
Depletion of endogenous iPLA2 β sensitizes tumor cells to ROS-induced ferroptosis and enhances p53-dependent tumor growth suppression in xenograft mouse models. To investigate the role of iPLA2 β in modulating p53 functions, we first examined whether RNAi-mediated knockdown of endogenous iPLA2 β affects p53-dependent ferroptosis in human melanoma A375 cells. To this end, both A375 and isogenic p53-null A375 cells were transfected with siRNAs (Dharmacon SMART-pools) specific for iPLA2 β . Western blot analysis revealed that siRNA-mediated iPLA2 β depletion did not affect the expression levels of p53 or its transcriptional target p21 (Fig. 5a). As expected, p53-mediated ferroptosis was readily induced in TBH-treated cells transfected with control siRNAs (Fig. 5b). However, the levels of ferroptosis were significantly increased by iPLA2 β depletion in wild-type p53 (Fig. 5b), but no significant effect was observed in p53-null cells under the same conditions (Fig. 5b), suggesting that iPLA2 β can suppress p53-mediated ferroptosis. Similar results were also obtained in U2OS cells and isogenic p53-null U2OS cells by the same methods (Supplementary Fig. 5a, b). Previously, we showed that MCF7 human breast carcinoma cells are susceptible to p53-mediated ferroptosis¹¹ but, owing to a lack of ACSL4 expression, they are resistant to ferroptosis induced by either direct (e.g., RSL-3) or indirect (erastin) GPX4 inhibitors^{11,20}. As shown in Fig. 5c, iPLA2 β knockdown significantly enhanced p53-mediated ferroptosis in MCF7 cells (the levels of iPLA2 β were showed in Supplementary Fig. 6a). To further validate the role of iPLA2 β in p53-mediated ferroptosis, we used CRISPR/Cas9 technology to inactivate the iPLA2 β gene in A375 cells. Consistent with the above data, loss of iPLA2 β expression had no obvious effect on p53 levels and p53 transcriptional function (Fig. 5d) but p53-mediated ferroptosis was significantly elevated in iPLA2 β -null cells at different time points (Fig. 5e and Supplementary Fig. 6b, c). Likewise, p53-mediated ferroptosis was markedly enhanced by iPLA2 β depletion in U2OS cells (Fig. 6f and Supplementary Fig. 6d). Collectively, these data demonstrate that loss of iPLA2 β expression significantly sensitizes these cancer cells to p53-dependent ferroptosis upon ROS-induced stress.

To elucidate the physiological significance of iPLA2 β in ferroptosis regulation, we tested whether loss of iPLA2 β expression affects tumor growth in xenograft tumor models. Indeed, the growth of human melanoma A375 xenograft tumors was dramatically reduced upon inactivation of iPLA2 β expression (2 vs. 1, Fig. 6a, b) in xenograft tumor growth assays; however, the tumor suppressive effects induced by loss of iPLA2 β expression

were largely abrogated when isogenic p53-null A375 cells were used (4 vs. 3, Fig. 6a, b). Notably, upregulation of *Ptgs2*, a marker of ferroptosis, was observed in iPLA2 β ^{-/-} tumor samples but not in iPLA2 β ^{-/-}/p53^{-/-} samples (Fig. 6c). Finally, to further validate these observations, we performed a series of the similar experiments described above in human lung carcinoma A549 cells. Again, loss of iPLA2 β significantly enhanced p53-mediated ferroptosis (Fig. 6d and Supplementary Fig. 7). More importantly, inactivation of iPLA2 β also promoted the tumor suppressive effects in p53-WT cells but not isogenic p53-null cells (Fig. 6e–g). Taken together, these data demonstrate that the inhibition of iPLA2 β expression significantly enhances p53-mediated ferroptosis and that activation of ferroptosis by loss of iPLA2 β , at least, in part contributes to p53-dependent tumor growth suppression in vivo.

iPLA2 β downregulates the levels of peroxidized membrane lipids induced by ROS exposure and effectively suppresses p53-driven ferroptosis. Recent studies indicate that oxidized PUFA-containing phospholipids, but not free oxidized PUFAs, act as key executioners of ferroptosis²¹. The calcium-independent phospholipase family enzymes are known for their abilities to cleave acyl tails from the glycerol backbone of lipids and release oxidized fatty acids such as PUFAs, from membrane phospholipids^{23–26}. Thus, it is very likely that iPLA2 β suppresses ferroptosis by cleaving peroxidized lipids for detoxification. Since ALOX12 is required for p53-mediated ferroptosis upon ROS stress¹¹, we first examined whether ALOX12 expression can promote lipid peroxidation upon ROS-induced stress and whether the levels of the oxidized phospholipids induced by ALOX12 are suppressed by iPLA2 β . To this end, U2OS cells were transfected with expression vectors encoding ALOX12 alone or both ALOX12 and iPLA2 β (Fig. 7a), stained with C11-BODIPY, and analyzed by flow cytometry to assess levels of endogenous lipid peroxidation from cell membrane. As shown in Fig. 7b, c, peroxidized lipid levels were markedly increased by ALOX12 expression; however, these elevated levels were effectively reduced upon co-expression of iPLA2 β . As expected, iPLA2 β expression also reduced the levels of ferroptosis induced by ALOX12 expression (Supplementary Fig. 8). These data indicate that iPLA2 β can suppress ferroptosis by abrogating ALOX12-induced lipid peroxidation.

Since p53-mediated ferroptosis is independent of GPX4 (Fig. 1d), we examined whether iPLA2 β can also modulate p53-mediated ferroptosis in GPX4-null cells. To this end, we transfected ACSL4/GPX4-null U2OS cells with expression vectors encoding either iPLA2 β or, iPLA2 γ as an additional control (Fig. 7d), and analyzed lipid peroxidation levels by flow cytometry with C11-BODIPY staining. As shown in Fig. 7e, the elevated levels of lipid peroxidation induced by p53 activation under ROS stress in ACSL4/GPX4-null cells (I) were significantly reduced by expression of iPLA2 β (II), but not by iPLA2 γ expression (III, Fig. 7e). Moreover, p53-mediated



ferroptosis was completely abrogated by overexpression of iPLA2 β but not by iPLA2 γ expression in these GPX4-null cells (Fig. 7f). Thus, iPLA2 β suppresses p53-mediated ferroptosis by reducing the levels of lipid peroxidation in a GPX4-independent manner.

Next, we performed targeted lipidomics to monitor the levels of peroxidized lipids regulated by iPLA2 β . Indeed, the levels of the oxidized phosphatidylethanolamine (PE) and phosphatidylcholine (PC) (oxPE (18:0/22:4)sn2 or oxPC (18:0/20:4)sn2) were

Fig. 6 iPLA2 β acts as a major suppressor of p53-mediated tumor suppressor. **a** Xenograft tumors from A375 CRISPR control, iPLA2 $\beta^{-/-}$, p53 $^{-/-}$ or p53 $^{-/-}$; iPLA2 $\beta^{-/-}$ cells as indicated. **b** Tumor weights were determined from **(a)** (error bars, from eight tumors). The experiments were repeated twice independently with similar results and representative data were shown. $p = 0.00049$ for control versus iPLA2 $\beta^{-/-}$; $p = 0.469$ for p53 $^{-/-}$ versus iPLA2 $\beta^{-/-}$; $p53^{-/-}$. **c** qPCR of *Ptgs2* mRNA from tumors harvested in **(a)**. $p = 0.00349$ for control versus iPLA2 $\beta^{-/-}$. **d** A549 cells (Lanes 1, 2), p53 $^{-/-}$ cells (lanes 3, 4), iPLA2 $\beta^{-/-}$ cells (lanes 5, 6), or p53 $^{-/-}$; iPLA2 $\beta^{-/-}$ cells (lanes 7, 8) treated with Nutlin 10 μM for 24 h (lanes 2, 4, 6, 8) versus control (lanes 1, 3, 5, 7) by the antibodies to iPLA2 β , p53, p21 or actin. The experiments were repeated twice, independently, with similar results. **e** Xenograft tumors from A549 CRISPR control, iPLA2 $\beta^{-/-}$, p53 $^{-/-}$ or p53 $^{-/-}$; iPLA2 $\beta^{-/-}$ cells as indicated. **f** Tumor weights were determined from **(e)** (error bars, from eight tumors). The experiments were repeated twice independently with similar results and representative data were shown. $p = 0.00253$ for A549 versus iPLA2 $\beta^{-/-}$; $p = 0.686$ for p53 $^{-/-}$ versus iPLA2 $\beta^{-/-}$; p53 $^{-/-}$. **g** qPCR of *Ptgs2* mRNA from tumors harvested in **(e)**. $p = 0.00000727$ for A549 versus iPLA2 $\beta^{-/-}$. **b, f** Error bars are mean \pm SEM. **c, g** Error bars are mean \pm s.d., **b-c, f-g** $n = 8$ biologically independent samples. All p values were calculated using two-tailed unpaired Student's t -test. Detailed statistical tests are described in the 'Methods'. Source data are provided as a Source Data file.

significantly induced upon ALOX12 expression, indicating that ALOX12 is critical for generating oxidized PE and oxidized PC in human cancer cells (Fig. 7g, h and Supplementary Fig. 9a–c). However, the increased levels of the oxidized phosphatidylethanolamine (PE) and phosphatidylcholine (PC) (oxPE (18:0/22:4)sn2 or oxPC (18:0/20:4)sn2) were dramatically reduced upon expression of iPLA2 β but not the enzymatic defective mutant iPLA2 β (G517C) (Fig. 7g, h and Supplementary Fig. 9a, b). Consistent with these observations, this enzymatic defective mutant iPLA2 β (G517C) also failed to suppress p53-mediated ferroptosis (Fig. 7i). These data demonstrate that both ALOX12 and iPLA2 β play critical roles in directly regulating the levels of the oxidized phosphatidylethanolamine (PE) and phosphatidylcholine (PC) during ferroptotic responses.

Finally, two recent studies have identified FSP1 (ferroptosis suppressor protein 1) as another important regulator for ferroptosis induced by GPX4 inhibitors^{28,29}. The FSP1–CoQ₁₀–NAD(P)H pathway exists as a parallel system, which co-operates with GPX4 and glutathione to suppress phospholipid peroxidation and ferroptosis. To examine whether iPLA2 β -mediated effects on ferroptosis can be induced independent of FSP1 function, we generated FSP1 derivatives of the human osteosarcoma cell line U2OS. As expected, these FSP1-null cells are more sensitive to ferroptosis induced by the GPX4 inhibitor RSL-3 (Supplementary Fig. 10). Nevertheless, p53-mediated ferroptosis was readily induced in FSP1-null cells and more importantly, the cell death was effectively suppressed by iPLA2 β in those cells (Fig. 8a, b). Together, these data demonstrate that iPLA2 β -mediated effects on ferroptosis are completely independent of GPX4 or FSP1.

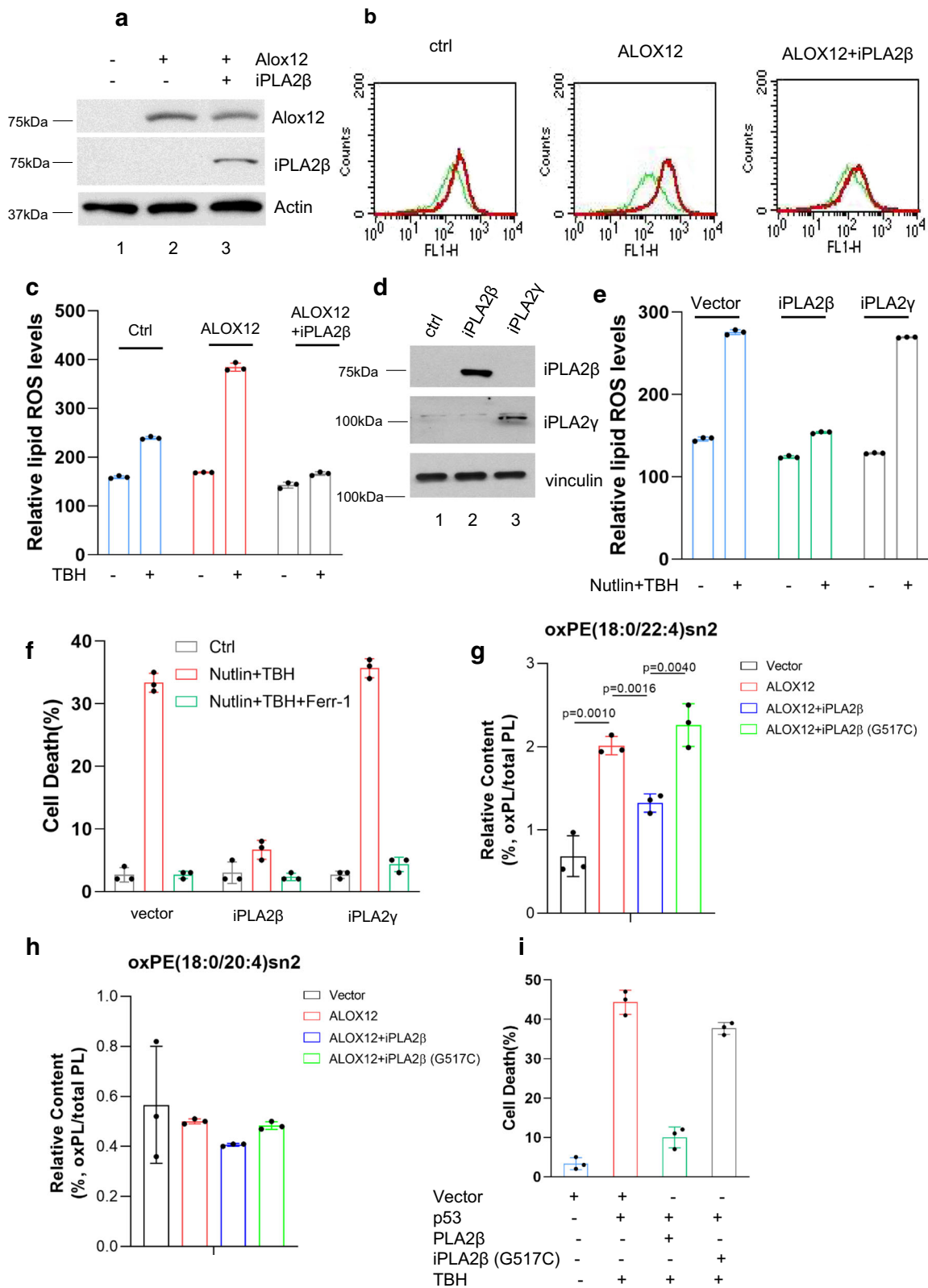
Discussion

Our results indicate that iPLA2 β -mediated lipid detoxification is critical for suppressing ROS-induced ferroptosis in cancer cells. By using mouse tumor models, we and others previously showed that p53-mediated ferroptosis acts as a new tumor suppression mechanism independent of the classic mechanisms such as cell cycle arrest, apoptosis, and senescence^{7,8,10,22}. Thus, at first glance, it might seem surprising that p53 can activate transcription of the iPLA2 β gene, which encodes a potent suppressor of p53-mediated ferroptosis. Yet, in this regard, there are intriguing parallels between the manner in which p53 regulates apoptosis and ferroptosis. Previous studies have established that p53 induces apoptosis under conditions of high stress by transactivation of apoptotic effector genes, such as PUMA and NOXA³⁰. However, under low-stress conditions, p53 can instead transactivate expression of the pro-survival genes such as TIGAR, which protects cells from apoptosis²⁷. Thus, by differentially regulating both pro- and anti-apoptotic gene, p53 can ensure that apoptosis ensues only when the cell death becomes inevitable (e.g., the damage is unreparable). Indeed, p53-mediated activation of

iPLA2 β is only observed at the early stage of stress responses or under low levels of stress but this activation is diminished at the late stage of stress responses or under high levels of stress. Similar to the effects on tumor development by loss of TIGAR³¹, inactivation of iPLA2 β enhances the tumor suppressive effects of p53. Thus, like TIGAR, iPLA2 β may help cells to survive transient or under low levels of stress; however, under high levels of stress or at the late stage of the stress responses, p53-mediated activation of iPLA2 β is abrogated and high levels of ferroptotic responses are designed to effectively eliminate the damaged cells (Fig. 8c).

Although iPLA2 β and GPX4 both modulate ferroptosis by detoxifying lipid peroxides, each does so in a biochemically distinct manner: while GPX4 protects cells from ferroptosis by converting oxidized phospholipids into non-toxic lipid alcohols, iPLA2 β suppresses ferroptosis by cleaving peroxidized lipids for detoxification. The existence of two distinct lipid repair mechanisms raises interesting questions regarding their different physiological functions. The physiological significance of GPX4 in regulating ferroptosis is best illustrated by the severe phenotypes associated with *Gpx4*-mutant mice^{32–35}. For example, while *Gpx4*-null mice undergo early embryonic lethality³², studies of conditional *Gpx4*-mutant mice show that GPX4 loss also elicits cell death in multiple adult tissues³³. Moreover, under normal conditions, most cell lines cannot be successfully cultured in the absence of GPX4²⁰. In contrast, we have successfully established iPLA2 $\beta^{-/-}$ cell lines and grew these cells under normal conditions without any difficulty. Moreover, the iPLA2 β gene is not required for embryonic development or normal cell homeostasis. Indeed, iPLA2 $\beta^{-/-}$ mice develop normally and grew to maturity^{36,37}. Thus, it seems likely that GPX4 and iPLA2 β regulate ferroptosis in different physiological settings. On one hand, *Gpx4* may serve as a 'housekeeping' gene that controls the levels of lipid peroxidation under conditions of normal homeostasis. On the other hand, iPLA2 β is not required for ferroptotic responses under normal homeostasis conditions but is critical for controlling lipid peroxidation levels and ferroptosis during stress responses (Fig. 8c).

The precise mechanism by which iPLA2 β -mediated repression of ROS-induced ferroptosis contributes to cancer development needs further elucidation. Through expression profile analysis of iPLA2 β from the cancer databases, we found that iPLA2 β is overexpressed in many human cancers including kidney renal clear cell carcinoma (RCC) and acute myeloid leukemia (AML) (<https://www.cbioportal.org/>); more importantly, the cancer patients expressing higher levels of iPLA2 β have a significantly shorter overall survival (Fig. 8d, e). Although the p53 gene is frequently mutated (more than 50%) in most of human cancers, the mutation rate of p53 is very low in either RCCs or AMLs (<https://p53.iarc.fr>). Thus, these data suggest that repression of p53-dependent ferroptosis by iPLA2 β may play an important role in tumor development of these cancers. Notably, cancer cells



rewire cellular metabolism to meet the energetic and substrate demands of tumor development, but this rewiring also creates metabolic vulnerabilities specific for cancer cells³⁸. To fuel their enhanced growth and proliferation, cancer cells undergo metabolic reprogramming, generally accompanied by increased ROS production^{38,39}. Thus, the levels of ROS are much higher in cancer cells than in normal cells, making the cancer cells more

susceptible to ROS-induced ferroptosis. Given that loss of iPLA2β, in contrast to GPX4, does not affect normal development or cell viability in normal tissues but iPLA2β plays an essential role in ROS-induced ferroptosis in tumor cells, we propose iPLA2β as a more promising therapeutic target than GPX4 for activating ferroptosis in human cancers without causing severe toxicity.

Fig. 7 Mechanistic insights into iPLA2 β -mediated suppression of lipid peroxidation and ferroptosis induced by p53 and ROS stress. **a** Western blot analysis of U2OS ACSL4 $^{-/-}$; GPX4 $^{-/-}$ cells transfected with ALOX12 or iPLA2 β vector. The experiments were repeated twice, independently, with similar results. **b** Lipid peroxidation levels of U2OS ACSL4 $^{-/-}$; GPX4 $^{-/-}$ cells transfected with ALOX12 or iPLA2 β vector were treated with TBH (300 μ M) and Ferr-1 (2 μ M) as indicated for 8 h. **c** Quantification of lipid peroxidation levels as shown in (b). Error bars are mean \pm s.d., $n = 3$ independent experiments. **d** Western blot analysis of U2OS ACSL4 $^{-/-}$; GPX4 $^{-/-}$ cells transfected with iPLA2 β or iPLA2 γ vector. The experiments were repeated twice, independently, with similar results. **e** Quantification of lipid peroxidation levels. U2OS ACSL4 $^{-/-}$; GPX4 $^{-/-}$ cells with overexpression of iPLA2 β or iPLA2 γ were pre-incubated with Nutlin (10 μ M) for 12 h, then treated with TBH (300 μ M) and Nutlin (10 μ M) as indicated for 8 h. **f** Quantification of cell death. U2OS ACSL4 $^{-/-}$; GPX4 $^{-/-}$ cells with overexpression of iPLA2 β or iPLA2 γ were pre-incubated with Nutlin (10 μ M) for 24 h, then treated with TBH (250 μ M) and Nutlin (10 μ M) as indicated. **g** Relative content of oxPE (18:0/22:4)sn2 in H1299 cells transfected with alox12, or/and iPLA2 β (PE, phosphatidylethanolamines). p values were calculated using two-tailed unpaired Student's t -test. Detailed statistical tests are described in the 'Methods'. **h** Relative content of oxPE (18:0/20:4)sn2 in H1299 cells transfected ALOX12, or/and iPLA2 β . **i** Quantification of cell death in H1299 cells transfected with vector, p53, iPLA2 β WT or G517C, and additional TBH treatment. **e-i** Error bars are mean \pm s.d., $n = 3$ biologically independent experiments. Source data are provided as a Source Data file.

Methods

Cell culture and stable lines. U2OS, H1299, A375, MCF7, and A549 cancer lines were ordered from American Type Culture Collection (ATCC) and have been proven to be negative for mycoplasma contamination. All cell lines used in this work were not listed in the ICLAC database. Cells were always cultured in a 37 °C incubator with 5% CO₂. Media used for cells were supplemented in DMEM with 10% FBS, 100 U/mL penicillin and 100 μ g/mL streptomycin (all from Gibco). To obtain iPLA2 β , CRISPR-cas9-knockout U2OS cells were generated by transfecting iPLA2 β double nickase plasmid (sc-402107-NIC; Santa Cruz). Identical strategies were used to generate p53-knockout A375 cells (p53, sc-416469-NIC), iPLA2 β or both p53- and iPLA2 β -knockout A375 cells. The cells were selected with puromycin (1 μ g/mL) for 4–6 days. iPLA2 β , p53-knockout, or both iPLA2 β - and p53-knockout single clones were then screened and acquired after continuing to culture 2–3 weeks without selective antibiotics. p53 CRISPR-knockout, alox12-knockout, ACSL4 and GPX4-knockout U2OS cells have been described previously¹¹. For FSP1 CRISPR U2OS cells, CRISPR guide RNA (sgRNA) sequences targeting FSP1 5' caccgGAATCGGGAGCTCTGCACG 3' (22) was synthesized by Invitrogen. Lipofectamine[®]CRISPRMAX were used for transfection following manufacturer's protocol (Invitrogen). Individual clone of U2OS for FSP1 $^{-/-}$ was confirmed by western blot.

Plasmids. Full-length iPLA2 β cDNA from Korolev lab (Saint Louis University)⁴⁰, was subcloned into pcDNA3.1/v5-His-Topo vector (Invitrogen). To prepare mutant construct iPLA2 β , cDNA sequences corresponding to the region was amplified by PCR from above constructs using QuikChange Site-Directed Mutagenesis Kit (Stratagene) and subcloned into pcDNA3.1/v5-His-Topo vector. GFP-ipla2 γ plasmid was generously gifted from Cybulsky lab (McGill University)⁴¹. p53 WT and its mutant plasmids (R175H, R248W, and R273H) have been described previously⁹.

Western blotting and antibodies. Protein extracts were blotted by Western according to standard protocols using primary antibodies specific for p53 (sc126, DO-1; Santa Cruz, 1:1000 dilution), iPLA2 β (sc376563, D-4, Santa Cruz, 1:200 dilution), MDM2 (SRP2095, Ab5; Millipore, 1:500 dilution), p21 (C-19; Santa Cruz, 1:400 dilution), ACSL4 (sc-271800; Santa Cruz, 1:1000 dilution), GPX4 (ab125066; Abcam, 1:500 dilution), V5 (46-0725; Invitrogen, 1:500 dilution), ALOX12 (sc-365194; Santa Cruz, 1:200 dilution), AMID (FSP1) (sc-377120; Santa Cruz, 1:400 dilution), SLC7A11 (D2M7A) (12691 s; Cell Signaling, 1:500 dilution), Vinculin (V9264; Sigma-Aldrich, 1: 5000 dilution), Actin (A3853; Sigma-Aldrich, 1:5000 dilution), GFP (565271; BD Biosciences, 1:1000 dilution), and TIGAR (sc-166290, Santa Cruz, 1:500 dilution). HRP-conjugated anti-mouse (111-035-146, Jacksonimmuno, 1:500 dilution), and HRP-conjugated anti-rabbit (111-035-045, Jacksonimmuno, 1:500 dilution) secondary antibodies were used.

Ablation of endogenous iPLA2 β by RNAi. Knockdown of iPLA2 β protein was performed by transfection of U2OS, A375, and MCF-7 cells with siRNA duplex oligo (ON-TARGET plus SMARTpool: L-00908; Dharmacon) by Lipofectamine 3000 (Invitrogen) for 24 h and then transfected again according to the manufacturer's protocol.

RNA extraction and qRT-PCR. Total RNA was isolated using TRIzol (Invitrogen) according to the manufacturer's protocol. cDNA was reversed by SuperScript[™] IV VILO[™] Master Mix (Invitrogen). For the qRT-PCR analysis, the following primers were used: human iPLA2 β forward 5'-GCAATGCTCGGTGCAACAT-3', iPLA2 β reverse 5' - ACACCCCTTCTGAGAGAAGCTTCA-3'; human HPRT forward, TATGGCGACCCGAGCCCT, HPRT reverse, CATCTCGAGCAAGACGTTTCAG (also see Supplementary Table 1).

Chromatin immunoprecipitation assay. The assay was performed as described previously with a little modifications⁷. In short, cells were crosslinked with 1% formaldehyde for 10 min at room temperature and neutralized with a final concentration of 0.125 M glycine. The harvested cells were suspended in cold lysis buffer (10 mM Tris-Cl, pH8.0, 85 mM KCl, 0.25% triton, 0.5% NP40, 5 mM EDTA and protease inhibitor mixture). After 10 min incubation at 4 °C, nuclei were harvested and lysed in CHIP buffer (50 mM Tris-HCl pH 8.0, 1% SDS, 5 mM EDTA and protease inhibitor mixture). After sonication, the lysates were centrifuged, the supernatants were added with magnetic beads coated with the specific p53 antibody (full length 393, Santa Cruz) and incubated overnight. Beads were washed seven times with washing buffer (50 mM HEPES, pH7.5, 1 mM EDTA, 500 mM HCl, 0.7% Na-deoxycholate and 1% NP40) and once with TE buffer before the protein-DNA complex was eluted with 0.1 M NaHCO₃ and 1% SDS. After reverse crosslinking overnight at 55 °C, DNA was extracted and qPCR performed. iPLA2 β primers: RE1 forward 5'-GCCGGCTCTGTATCTCTCAA-3', reverse 5'-ACCGAATGACCTGGGAAGG-3'; RE2 forward 5'-CCTCTGCCTTC TGGGCTAA-3', reverse 5'-ACATGGTGAAACCCCATCTC-3'; RE3 forward 5'-GC ATCACTGGTCTCTGTCCG-3', reverse 5' GTCTAAAATGGGGTTCTGCT-3'. TIG AR primers: forward 5'-CGGCAGGCTTATAGATAGCTT-3', reverse 5'-GGCAGCCG GCATCAAAAACA-3' (also see Supplementary Table 1).

Cell death assay. For cell death assays^{7,9,11,42}, cells were trypsinized, collected and stained with trypan blue. The cells were counted with a hemocytometer using the standard protocol, and cells stained blue were considered as dead cells. The cell death was further confirmed by propidium iodide staining followed by FACS analysis. For CellTiter-Glo luminescent assay⁴³, 10⁴ cells were plated 90 μ L per well of a 96-well plate on day 1. The treatments were added to each well of the plates on day 2. The viability of cells was measured using 1:1 dilution of the CellTiter-Glo luminescent reagent (Promega G7572), which was read on a Glomax explorer (Promega) after 10 min of shaking at room temperature. The intensity of luminescence was normalized to that of DMSO control. Percentage of Cell death was counted as 100 minus percentage of cell viability.

Mouse xenograft. Six weeks old female nude mice (NU/NU, Charles River) were used. All the mice were housed in a temperature controlled room (65–75 °F) with 40–60% humidity, with a light/dark cycle of 12 h/12 h. Mice weights were about 24.7 \pm 1.77 g. 2.0 \times 10⁶ of A375 or A549 CRISPR control, p53 $^{-/-}$, iPLA2 β $^{-/-}$, or p53 $^{-/-}$; iPLA2 β $^{-/-}$ cells were mixed with Matrigel (BD Biosciences) at 1:1 ratio (volume) and injected subcutaneously into nude mice. The mice were killed 20 days for A375, or 30 days for A549 cells after injection and the weight of the tumors was measured and recorded. Every experimental protocol was approved by the Institutional Animal Care and Use Committee (IACUC) of Columbia University (AAAW1456). The tumors in the experiments did not exceed the limit for tumor burden (10% of total body weight or 2 cm in diameter).

Drugs and inhibitors. For ROS generation, *tert*-Butyl hydroxide solution (TBH, Sigma), butanone peroxide (BTP, Sigma), or cumene hydroperoxide (CMH, Sigma) was used as seen in respective figure legends. Specific cell-death inhibitors were used in the experiments at the following concentrations: Ferrostatin-1 (ferroptosis inhibitor; Xcess Biosciences), 2 μ M; Z-VAD-fmk (Pan-caspase inhibitor; Sigma), 10 μ g/mL; Necrostatin-1 (necroptosis inhibitor; Sigma), 10 μ g/mL; 3-MA (autophagy inhibitor; Sigma), 2 mM.

Lipid ROS assay using flow cytometer. Lipid ROS assay was performed as described previously¹¹. Briefly, cells were incubated with DMEM containing 5 μ M of C-11 BODIPY dye in tissue culture incubator for 30 min. Cells were then collected by trypsinization, and washed twice with PBS followed by re-suspending in 500 μ L of PBS. Lipid ROS levels were analyzed using a Becton Dickinson FACS-Calibur machine through the FL1 channel. In all, 10,000 cells were analyzed using CellQuest in each sample.

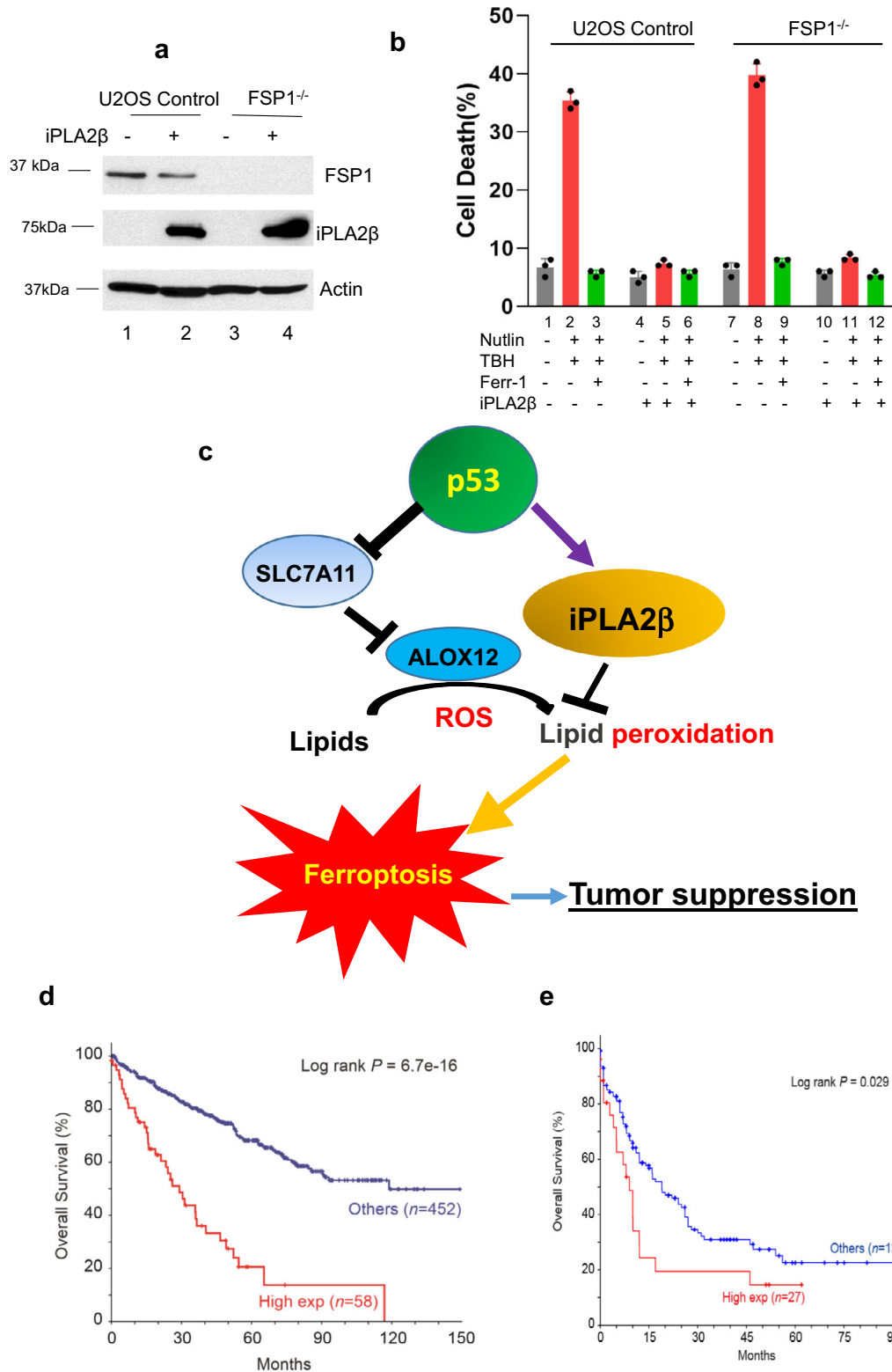


Fig. 8 The roles of ALOX12 and iPLA2β in regulating p53-mediated ferroptosis. **a** Western blot analysis of extracts of U2OS CRISPR control (lanes 1, 2) or FSP1^{-/-} cells (lanes 3, 4) with overexpression of iPLA2β-V5 (lanes 2, 4) versus empty vector (lanes 1, 3) by the antibodies to FSP1, V5, or actin. The experiments were repeated twice, independently, with similar results. **b** Quantification of cell death in the same cells as (**a**) treated with 250 μM TBH after pretreatment with Nutlin 10 μM for 24 h. Error bars are mean ± s.d., $n = 3$ biologically independent experiments. **c** A model for the roles of ALOX12 and iPLA2β in regulating p53-mediated ferroptosis. **d** Kaplan-Meier survival curve was generated for overall survival by stratifying patient samples with kidney renal clear cell carcinoma (TCGA, PanCancer Atlas) from cBioPortal based on iPLA2β expression levels. High-expression group was defined as mRNA expression z-score > 1 (PLA2G6: EXP > 1). **e** Kaplan-Meier survival curve was generated for overall survival by stratifying patient samples with acute myeloid leukemia (TCGA, PanCancer Atlas) from cBioportal based on iPLA2β expression levels. **d, e** p values were calculated using two-sided unpaired Student's t -test. Detailed statistical tests are described in the 'Methods'. Source data are provided as a Source Data file.

LC-MS/MS-based analysis of oxidized phospholipids. H1299 cells were transfected ALOX12 alone or co-transfected ALOX12 plus iPLA2 β or iPLA2 β enzymatic deficit mutant with three biological replicates. One day after transfection, 1 million cells were trypsinized, washed, and collected in cryogenic vials. Vials were stored at liquid nitrogen until the time of analysis. The cell pellets were thawed on ice and added 500 μ L PBS/methanol 1:1 (v/v). Then 100 μ L methanol containing 50 ng each of the internal standards PC(15:0/18:1-d7), PE(15:0/18:1-d7) (EquiSPLASH, Avanti Polar Lipids). Samples were then transferred into 8 mL screw-cap tubes, and 1.125 mL methanol and 5 mL MTBE were added. After vigorous mixing, samples were incubated at room temperature on a tabletop shaker for 45 min. For phase separation, 1.25 mL water was added, and samples were vortexed and centrifuged for 15 min at 2000g. The upper organic phase of each sample was carefully removed using a Pasteur pipette, transferred into an empty glass round-bottom tube, and dried under vacuum in a SpeedVac concentrator. The dried lipid extracts were resuspended in 200 μ L HPLC mobile phase A/mobile phase B 3:1 (v/v) for targeted lipidomic analysis of oxidized phospholipids. 20 μ L samples were used for HPLC system (ExionLC Integrated System, Sciex)/Mass spectrometer (QTrap 6500+, Sciex) detection. Here is the index for HPLC: Column: Kinetex 2.6 μ m HILIC 100 \AA 100 \times 2.1 mm, Phenomenex; Flow Rate: 200 μ L/min. Total ion signals corresponding to all analytes and internal standards in the positive- and negative-ion modes. The specific precursor-product pairs monitored in negative-ion mode and used for quantification: PE(18:0/20:4), 766.5/303.2; PE(18:0/22:4), 794.6/331.2; PE(18:0/20:4-OH), 782.5/319.2; PE(18:0/20:4-OOH), 798.5/335.2; PE(18:0/22:4-OH), 810.6/347.2; PE(18:0/22:4-OOH), 826.6/363.2; PC(18:0/20:4), 868.6/303.2; PC(18:0/22:4), 896.6/331.2; PC(18:0/20:4-OH), 884.6/319.2; PC(18:0/20:4-OOH), 900.7/335.2; PC(18:0/22:4-OH), 912.6/347.2; PC(18:0/22:4-OOH), 928.6/363.2; PC(15:0/18:1-d7) internal standard, 753.6/184.1; PE(15:0/18:1-d7) internal standard, 711.6/570.3. The relative content of oxidized phospholipids was calculated by the ratio of hydroxyl group (-OH) and hydroperoxyl group (-OOH) to total phospholipids.

Data analysis and statistics. Data quantification was performed with Excel 2016, ImageJ 1.51W, and CellQuest Pro 6.0. Statistical analyses with Excel and GraphPad Prism V6. Images were processed by Adobe Photoshop. Results are shown as mean \pm s.d., except in Fig. 6b, f. Difference was determined by using a two-tailed, unpaired Student's *t*-test with a confidence interval (CI) of 95%. *p* < 0.05 was defined as statistically significant.

Reporting summary. Further information on research design is available in the Nature Research Reporting Summary linked to this article.

Data availability

The association of iPLA2 β with overall survival in patients with kidney renal clear cell carcinoma and acute myeloid leukemia were from cBioPortal for Cancer Genomics databases (<http://www.cbioportal.org>). All other data for the findings of this study are available from the corresponding author on reasonable request. Source data are provided with this paper.

Received: 16 April 2020; Accepted: 21 May 2021;

Published online: 15 June 2021

References

- Boutelle, A. M. & Attardi, L. D. p53 and tumour suppression: it takes a network. *Trends Cell Biol.* **31**, 298–310 (2021).
- Liu, Y., Tavana, O. & Gu, W. p53 Modifications: exquisite decorations of the powerful guardian. *J. Mol. Cell Biol.* **11**, 564–577 (2020).
- Karni-Schmidt, O., Lokshin, M. & Prives, C. The roles of MDM2 and MDMX in cancer. *Annu. Rev. Pathol.* **11**, 617–644 (2016).
- Mullard, A. p53 Programmes plough on. *Nat. Rev. Drug Discov.* **19**, 497–500 (2020).
- Humpton, T. & Vousden, K. H. Taking up the reins of power: metabolic functions of p53. *J. Mol. Cell Biol.* **11**, 610–614 (2019).
- Kastenhuber, E. R. & Lowe, S. W. Putting p53 in context. *Cell* **170**, 1062–1078 (2017).
- Jiang, L. et al. Ferroptosis as a p53-mediated activity during tumour suppression. *Nature* **520**, 57–62 (2015).
- Jennis, M. et al. An African-specific polymorphism in the TP53 gene impairs p53 tumor suppressor function in a mouse model. *Genes Dev.* **30**, 918–930 (2016).
- Ou, Y., Wang, S. J., Li, D., Chu, B. & Gu, W. Activation of SAT1 engages polyamine metabolism with p53-mediated ferroptotic responses. *Proc. Natl Acad. Sci. USA* **113**, E6806–E6812 (2016).
- Saint-Germain, E. et al. SOCS1 regulates senescence and ferroptosis by modulating the expression of p53 target genes. *Aging* **9**, 2137–2162 (2017).
- Chu, B. et al. ALOX12 is required for p53-mediated tumor suppression through a distinct ferroptosis pathway. *Nat. Cell Biol.* **21**, 579–531 (2019).
- Stockwell, B. R., Jiang, X. & Gu, W. Emerging mechanisms and disease relevance of ferroptosis. *Trends Cell Biol.* **30**, 478–490 (2020).
- Zhang, Y. L. et al. BAP1 links metabolic regulation of ferroptosis to tumour suppression. *Nat. Cell Biol.* **20**, 1181–1192 (2018).
- Xie, Y. et al. Ferroptosis: process and function. *Cell Death Differ.* **23**, 369–379 (2016).
- Angeli, J. P. F., Shah, R., Pratt, D. A. & Conrad, M. Ferroptosis inhibition: mechanisms and opportunities. *Trends Pharm. Sci.* **38**, 489–498 (2017).
- Yang, W. S. et al. Regulation of ferroptotic cancer cell death by GPX4. *Cell* **156**, 317–331 (2014).
- Liu, H., Schreiber, S. L. & Stockwell, B. R. Targeting dependency on the GPX4 lipid peroxide repair pathway for cancer therapy. *Biochemistry* **57**, 2059–2060 (2018).
- Viswanathan, V. S. et al. Dependency of a therapy-resistant state of cancer cells on a lipid peroxidase pathway. *Nature* **547**, 453–457 (2017).
- Hangauer, M. J. et al. Drug-tolerant persister cancer cells are vulnerable to GPX4 inhibition. *Nature* **551**, 247–250 (2017).
- Doll, S. et al. ACSL4 dictates ferroptosis sensitivity by shaping cellular lipid composition. *Nat. Chem. Biol.* **13**, 91–98 (2017).
- Kagan, V. E. et al. Oxidized arachidonic and adrenic PEs navigate cells to ferroptosis. *Nat. Chem. Biol.* **13**, 81–90 (2017).
- Wang, S. J. et al. Acetylation is crucial for p53-mediated ferroptosis and tumor suppression. *Cell Rep.* **17**, 366–373 (2016).
- Ramanadham, S. et al. Calcium-independent phospholipases A2 and their roles in biological processes and diseases. *J. Lipid Res.* **56**, 1643–1668 (2015).
- Liu, G. Y. et al. The phospholipase iPLA2 γ is a major mediator releasing oxidized aliphatic chains from cardiolipin, integrating mitochondrial bioenergetics and signaling. *J. Biol. Chem.* **292**, 10672–10684 (2017).
- Buland, J. R. et al. Biosynthesis of oxidized lipid mediators via lipoprotein-associated phospholipase A2 hydrolysis of extracellular cardiolipin induces endothelial toxicity. *Am. J. Physiol. Lung Cell Mol. Physiol.* **311**, L303–L316 (2016).
- Chao, H. et al. Disentangling oxidation/hydrolysis reactions of brain mitochondrial cardiolipins in pathogenesis of traumatic injury. *JCI Insight* **3**, e97677 (2018).
- Bensaad, K. et al. TIGAR, a p53-inducible regulator of glycolysis and apoptosis. *Cell* **126**, 107–120 (2006).
- Bersuker, K. et al. The CoQ oxidoreductase FSP1 acts parallel to GPX4 to inhibit ferroptosis. *Nature* **575**, 688–692 (2019).
- Doll, S. et al. FSP1 is a glutathione-independent ferroptosis suppressor. *Nature* **575**, 693–698 (2019).
- Kruiswijk, F., Labuschagne, C. F. & Vousden, K. H. p53 in survival, death and metabolic health: a lifeguard with a licence to kill. *Nat. Rev. Mol. Cell Biol.* **7**, 393–405 (2015).
- Cheung, E. C. et al. TIGAR is required for efficient intestinal regeneration and tumorigenesis. *Dev. Cell* **25**, 463–477 (2013).
- Imai, H. et al. Early embryonic lethality caused by targeted disruption of the mouse PHGPx gene. *Biochem. Biophys. Res. Commun.* **305**, 278–286 (2003).
- Angeli, J. P. F. et al. Inactivation of the ferroptosis regulator Gpx4 triggers acute renal failure in mice. *Nat. Cell Biol.* **16**, 1180–1120 (2014).
- Ingold, I. et al. Selenium utilization by GPX4 is required to prevent hydroperoxide-induced ferroptosis. *Cell* **172**, 409–422 (2018).
- Wortmann, M. et al. Combined deficiency in glutathione peroxidase 4 and vitamin E causes multiorgan thrombus formation and early death in mice. *Circ. Res.* **113**, 408–417 (2013).
- Otto, A. C. et al. Group VIA phospholipase A2 deficiency in mice chronically fed with high-fat-diet attenuates hepatic steatosis by correcting a defect of phospholipid remodeling. *Biochim. Biophys. Acta Mol. Cell Biol. Lipids* **1864**, 662–676 (2019).
- Bao, S. et al. Insulin secretory responses and phospholipid composition of pancreatic islets from mice that do not express Group VIA phospholipase A2 and effects of metabolic stress on glucose homeostasis. *J. Biol. Chem.* **281**, 20958–20973 (2006).
- Wolpaw, A. J. & Dang, C. V. Exploiting metabolic vulnerabilities of cancer with precision and accuracy. *Trends Cell Biol.* **28**, 201–212 (2018).
- Martinez-Outschoorn, U. E., Peiris-Pagés, M., Pestell, R. G., Sotgia, F. & Lisanti, M. P. Cancer metabolism: a therapeutic perspective. *Nat. Rev. Clin. Oncol.* **14**, 11–31 (2017).
- Malley, K. R. et al. The structure of iPLA2 β reveals dimeric active sites and suggests mechanisms of regulation and localization. *Nat. Commun.* **9**, 765 (2018).
- Elimam, H., Papillon, J., Takano, T. & Cybulsky, A. V. Complement-mediated activation of calcium-independent phospholipase A2 γ : role of protein kinases and phosphorylation. *J. Biol. Chem.* **288**, 3871–3885 (2013).
- Chen, D. et al. NRF2 is a major target of ARF in p53-independent tumor suppression. *Mol. Cell* **68**, 224–232 (2017).
- Venkatesh, D. et al. MDM2 and MDMX promote ferroptosis by PPAR α -mediated lipid-remodeling. *Genes Dev.* **34**, 526–543 (2020).

Acknowledgements

We thank Dr. Richard Baer for critical suggestions in this study. We also appreciate Dr. Sergey Korolev and Dr. Andrey V. Cybulsky for reagents. This work was supported by the National Cancer Institute of the National Institutes of Health under Award 5R01CA216884, 5R01CA190477, 5R01CA085533, 5R01CA254970, and 5R01CA224272 to W.G. and P01 CA087497, R35CA209896, and R61NS109407 to B.R.S. We acknowledge the support from the Herbert Irving Comprehensive Cancer Center (HICCC; P30 CA13696) and thank the Molecular Pathology and Proteomics of Shared Resources of HICCC. The content is solely the responsibility of the authors and does not necessarily represent the official views of the National Institutes of Health.

Author contributions

Conception and experimental design: D.C., B.C., and W.G. Methodology and data acquisition: D.C., B.C., X. Y., N.K., Y. J., Z.L., and R.R. Analysis and interpretation of data: D.C., B.C., and W.G. Manuscript writing: D.C., B.C., X.J., B.R.S., and W.G.

Competing interests

B.R.S. holds equity in and serves as a consultant to Inzen Therapeutics and is an inventor on patents and applications related to ferroptosis. The other authors declare no competing interests.

Additional information

Supplementary information The online version contains supplementary material available at <https://doi.org/10.1038/s41467-021-23902-6>.

Correspondence and requests for materials should be addressed to W.G.

Peer review information *Nature Communications* thanks the anonymous reviewer(s) for their contribution to the peer review of this work. Peer reviewer reports are available.

Reprints and permission information is available at <http://www.nature.com/reprints>

Publisher's note Springer Nature remains neutral with regard to jurisdictional claims in published maps and institutional affiliations.



Open Access This article is licensed under a Creative Commons Attribution 4.0 International License, which permits use, sharing, adaptation, distribution and reproduction in any medium or format, as long as you give appropriate credit to the original author(s) and the source, provide a link to the Creative Commons license, and indicate if changes were made. The images or other third party material in this article are included in the article's Creative Commons license, unless indicated otherwise in a credit line to the material. If material is not included in the article's Creative Commons license and your intended use is not permitted by statutory regulation or exceeds the permitted use, you will need to obtain permission directly from the copyright holder. To view a copy of this license, visit <http://creativecommons.org/licenses/by/4.0/>.

© The Author(s) 2021